IEEE PEDS 2019, Toulouse, France
9-12 July 2019

# Particle Swarm Optimization Tuning of MMCs in a Time-Invariant Framework

Gilbert Bergna-Diaz*, Andrea Formentini‡, Pericle Zanchetta‡ and Elisabetta Tedeschi*

*Dept. of Electric Power Engineering
Norwegian University of Science and Technology (NTNU)
Trondheim, Norway
{gilbert.bergna, elisabetta.tedeschi}@ntnu.no

‡Power Electronics, Machines and Control Group (PEMC)
The University of Nottingham - Nottingham
Nottingham, United Kingdom
{andrea.formentini, pericle.zanchetta}@nottingham.ac.uk

***Abstract*—This work investigates the Particle Swarm Optimization (PSO) algorithm as a tool to tune the control parameters of a Modular Multilevel Converter (MMC) in a single-terminal HVdc configuration. More precisely, due to its inherent capacity of handling system non-linearities, the PSO algorithm is used to tune a nonlinear control structure based on passivity arguments capable of ensuring global asymptotic stability of the converter. This nonlinear control strategy was successfully applied to the MMC in HVdc configuration in previous efforts, albeit with sub-optimal tuning, and therefore below par performance. Thus, this work aims to contribute to the state of the art by proving that system performance under the nonlinear control structure of interest can be further improved via PSO-tuning. Finally, to reduce the computational burden, we propose to apply the PSO algorithm directly to a recent state-space representation of an MMC with a constant equilibrium point.**

## I. Introduction

Multi-Terminal (MT) High-Voltage Direct-Current (HVdc) transmission systems are arguably one of the major infrastructure developments in this day and age, considered the preferred solution for integrating large volumes of renewable energy into the existing power grids, over very long distances [1]. Although two-level voltage source converters (2L-VSCs) have been traditionally used as the main component of MT-HVdc grids, attention has shifted to Modular Multilevel Converters (MMCs) [2], as the new preferred solution, mainly due to their reduced losses, modularity, scalability, low harmonic distortion and consequently reduced filtering requirements [3].

It is expected that the MMCs forming an MT-HVdc grid will need to guarantee a certain degree of *interoperability* between all the system components and associated controllers. In other words, stability and performance requirements of the overall interconnected system will need to be ensured. This becomes both, particularly important and challenging due to the expected multi-vendor nature of the system [4], as the local power converter controllers will usually be subjected to confidentiality agreements. A straightforward solution to overcome this problem is indeed relying on local controllers with *plug and play* features.

A possible approach for a *plug and play* stability guaranteed control design with simple PI controllers for the MMC was implemented in [5], [6], based on the passivity theory [7]–[10], and therefore extending to the MMC case the works of [11], [12] originally applied to 2L-VSCs. Nonetheless, even if global asymptotic stability was guaranteed, the controller in [5], [6] had sub-optimal tuning, and therefore below par performance. Thus, we are interested here in improving the tuning and consequently the performance of the nonlinear control applied to the MMC in [5], [6].

Towards this end, in this paper we investigate the potential of applying the Particle Swarm Optimization (PSO) algorithm [13], originally proposed in [14], to tune the MMC control parameters of the nonlinear control structure presented in [5], [6]. The PSO algorithm has been chosen due to its capability of handling system nonlinearities, its simple implementation and relatively low computational cost, compared to other methods [15], as well as its success in the power system community [16]. However, its heuristic nature still makes it computationally intensive. Therefore, it will be of interest to use a model able to reduce as much as possible the computational cost of the algorithm. Thus, this work is based on the steady-state time-invariant (SSTI) representation of the MMC proposed in [17], [18] which stabilizes at a *constant* equilibrium point instead of an oscillatory orbit. Using this equivalent state-space representation will allow for:

1) The use of efficient variable-step solvers; i.e., once the *constant* equilibrium is approached, the solver can use larger steps, decreasing the computational burden.
2) Initializing the converter variable at a constant equilibrium point, which in turns allow to apply the PSO tuning algorithm under an event of interest (e.g.: reference change) from the first iteration.
3) Simple inclusion of constant references in the objective function; as opposed to generating oscillatory references which are more computationally costly.

It is therefore proposed here as a suitable MMC model for tuning the control parameters by means of the PSO methodology.

The rest of the paper is organized as follows. In section II, the MMC average modelling conventions, as well as the equivalent model with time-invariant solutions proposed in [17] are briefly recalled. Section III gives a brief summary

978-1-5386-6499-5/19/$31.00 ©2019 IEEE

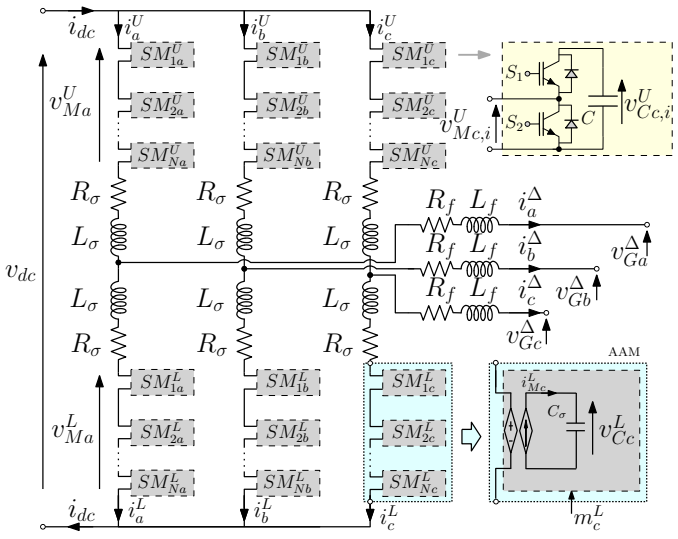


Fig. 1

Fig. 2: The MMC basic topology and arm average model representation (phase c).

of the PSO algorithm, while section IV outlines the control structure of interest applied to the MMC in [5]. In addition, time-domain simulation results of an MMC in single-terminal configuration with the control parameters tuned with the PSO methodology are given in section V.

## II. MMC Model in a Time-Invariant Framework

In this section, we briefly introduce the MMC structure with the adopted modelling conventions, and the steady-state time-invariant averaged model representation of [17].

### A. On the adopted modelling conventions

The basic topology of a three-phase MMC is displayed in Fig. 1. It is well known that the series connection of $N$ sub-modules (SMs) with capacitors $C$ constitute one arm of the converter. The arms are connected to a filter inductor with inductance $L_\sigma$ and equivalent resistance $R_\sigma$ to form the connection between one of the dc-terminals and the ac-side output. Two identical arms are connected to the upper and lower dc-terminals, respectively, to form one leg for each phase $j \in \{a, b, c\}$. The ac-side interface is assumed to be a filter inductor and/or the leakage inductance of a transformer, which is modeled by an equivalent inductance $L_f$ and resistance $R_f$. Assuming that the capacitor voltages of the sub-modules (SMs) are maintained well balanced within the converter arms, the series connection of SMs in each arm can be replaced by a circuit-based average model with $v_{C_j}^{U,L} = \sum_{i=1}^{N} v_{\mathrm{SM}j,i}^{U,L}$ and $C_\sigma = C/N$, (as indicated by the lower arm of phase $c$ in Fig. 1), corresponding to the average arm model (AAM) of the converter [19], [20].

The output of the controlled voltage sources of the AAM are referred to as the modulated voltages $v_{Mj}^U$ and $v_{Mj}^L$, respectively related to the equivalent arm capacitor voltages $v_{Cj}^U$ and $v_{Cj}^L$ by means of the equivalent insertion indices $m_j^U$ and $m_j^L$ through the relationships $v_{Mj}^U = m_j^U v_{Cj}^U$ and $v_{Mj}^L = m_j^L v_{Cj}^L$. Finally, $i_j^U$ and $i_j^L$ denote the upper and lower arm currents associated with $L_\sigma$, $i_j^\Delta$ the ac-grid current associated to $L_f$, and $v_{Gj}^\Delta$ the grid voltage at the ac side point of common coupling.

### B. Average model of the MMC in $\Sigma - \Delta$ representation

It was demonstrated in [17], [21], that it can be beneficial to adopt a Sum-Difference ($\Sigma$-$\Delta$) change of coordinates, instead of using the natural Upper-Lower ($U$-$L$) arm notation. Thus, the following definitions are introduced for a three phase MMC:

$$
\begin{aligned}
v_{Cabc}^\Sigma &:= v_{Cabc}^U + v_{Cabc}^L, \quad v_{Cabc}^\Delta := v_{Cabc}^U - v_{Cabc}^L \\
i_{abc}^\Sigma &:= \frac{1}{2}(i_{abc}^U + i_{abc}^L), \quad i_{abc}^\Delta := i_{abc}^U - i_{abc}^L \\
m_{abc}^\Sigma &:= m_{abc}^U + m_{abc}^L, \quad m_{abc}^\Delta := m_{abc}^U - m_{abc}^L,
\end{aligned}
$$

with $i_{abc}^\Sigma$ the circulating or common-mode currents, $i_{abc}^\Delta$ the ac-side grid currents; $v_{abc}^\Sigma$ and $v_{abc}^\Delta$ respectively the sum and difference between the upper and lower arm equivalent capacitor voltages; and $m_{abc}^\Sigma$ and $m_{abc}^\Delta$ the sum and difference between the upper and lower modulation indices. With such definitions, and by applying Kirchhoff's voltage and current laws to the circuit in Fig. 1, it is possible to represent the *average* converter dynamics as:

$$
\begin{aligned}
C_\sigma \dot{v}_{Cabc}^\Sigma &= m_{abc}^\Sigma \circ i_{abc}^\Sigma + \frac{1}{2} m_{abc}^\Delta \circ i_{abc}^\Delta; \\
C_\sigma \dot{v}_{Cabc}^\Delta &= m_{abc}^\Delta \circ i_{abc}^\Sigma + \frac{1}{2} m_{abc}^\Sigma \circ i_{abc}^\Delta; \\
L_\sigma \dot{i}_{abc}^\Sigma &= \frac{\mathbb{1}_3 v_{dc}}{2} - R_\sigma i_{abc}^\Sigma - \frac{m_{abc}^\Sigma \circ v_{Cabc}^\Sigma + m_{abc}^\Delta \circ v_{Cabc}^\Delta}{4}; \\
L_\delta \dot{i}_{abc}^\Delta &= -R_\delta i_{abc}^\Delta - \frac{m_{abc}^\Sigma \circ v_{Cabc}^\Delta + m_{abc}^\Delta \circ v_{Cabc}^\Sigma}{4} - v_{Gabc}^\Delta;
\end{aligned}
\tag{1}
$$

where $\circ$ denotes the Hadamard product (i.e., the element-wise multiplication of vectors), $\mathbb{1}_3 \in \mathbb{R}^3$ is a vector of ones, and $R_\delta \triangleq R_f + R_\sigma/2$ and $L_\delta \triangleq L_f + L_\sigma/2$ are the equivalent ac-side resistance and inductance, respectively.

### C. MMC model with time invariant solution

Finally, the equivalent SSTI representation is derived by applying the set of Park transformations $P_\omega$ and $P_{-2\omega}$, respectively at $\omega$, $-2\omega$; as well as a rotational transform $T_{3\omega}$ at $3\omega$ to the MMC state variables in a sum ($\Sigma$) and difference ($\Delta$) formulation, as sketched in Fig. 3—see [17] for a precise

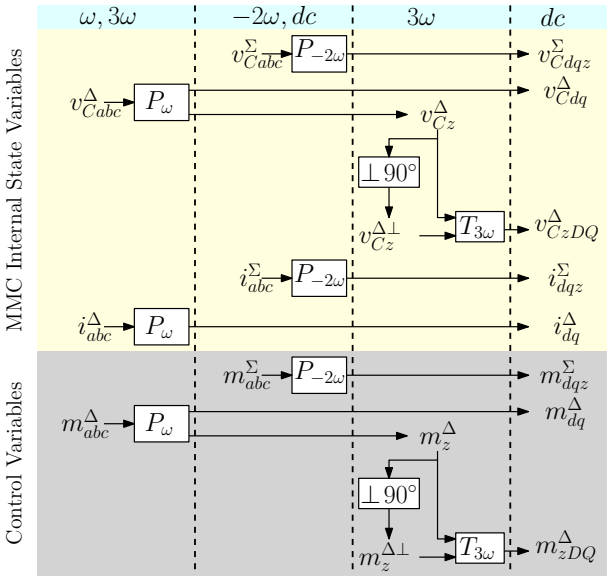


Fig. 3: Mapping of the MMC state variables proposed in [17] for a steady-state time-invariant dynamic equivalent state-space representation.

justification and detailed derivation. The model then reads:

$$\begin{aligned}
C_\sigma \dot{v}^{\Sigma}_{Cdq} &= \; i^{\Sigma}_{Mdq} + \mathbb{J}_2 C_\sigma 2\omega v^{\Sigma}_{Cdq},\\
C_\sigma \dot{v}^{\Sigma}_{Cz} &= \; i^{\Sigma}_{Mz},\\
C_\sigma \dot{v}^{\Delta}_{Cdq} &= \; i^{\Delta}_{Mdq} + \mathbb{J}_2 C_\sigma \omega v^{\Delta}_{Cdq},\\
C_\sigma \dot{v}^{\Delta}_{CzDQ} &= \; i^{\Delta}_{MzDQ} + \mathbb{J}_2 C_\sigma 3\omega v^{\Delta}_{CzDQ},\\
L_\sigma \dot{i}^{\Sigma}_{dq} &= -v^{\Sigma}_{Mdq} + (\mathbb{J}_2 L_\sigma 2\omega - R_\sigma \mathbb{I}_2) i^{\Sigma}_{dq},\\
L_\sigma \dot{i}^{\Sigma}_{z} &= -v^{\Sigma}_{Mz} - R_\sigma i^{\Sigma}_{z} + \frac{1}{2} v_{dc},\\
L_\delta \dot{i}^{\Delta}_{dq} &= \; v^{\Delta}_{Mdq} + (\mathbb{J}_2 L_\delta \omega - R_\delta \mathbb{I}_2) i^{\Delta}_{dq} - v^{\Delta}_{Gdq},
\end{aligned} \tag{2}$$

with $i^{\Sigma}_{Mdq}$, $i^{\Sigma}_{Mz}$, $i^{\Delta}_{Mdq}$, $i^{\Delta}_{MzDQ}$, $v^{\Sigma}_{Mdq}$, $v^{\Sigma}_{Mz}$ and $v^{\Delta}_{Mdq}$ the new modulated currents and voltages in $\Sigma$-$\Delta$ representation and $dqz$ (steady-state time-invariant) coordinates, defined in the appendix; and

$$\mathbb{J}_2 \triangleq \begin{bmatrix} 0 & -1 \\ 1 & 0 \end{bmatrix}.$$

**Remark 1.** Let the zero sequence of a general $\Delta$ variable be denoted as $x^{\Delta}_{z}$—examples of such variables include the zero-sequence of the voltage difference $v^{\Delta}_{Cz}$, the modulated current $i^{\Delta}_{Mz}$ and the zero sequence of the insertion indices difference $m^{\Delta}_{z}$. As detailed in [17], these variables do not reach a constant value in steady state, but a periodic orbit at $3\omega$ instead. Thus, it was proposed in [17] to use an auxiliary virtual variable $x^{\Delta\perp}_{z}$, $90°$ phase-shifted from $x^{\Delta}_{z}$ and define the new pair of *steady-state time-invariant* variables $x^{\Delta}_{zDQ} \triangleq T_{3\omega}\mathrm{col}(x^{\Delta}_{z}, x^{\Delta\perp}_{z})$, as partly sketched in Fig. 3.

**Remark 2.** It is worth mentioning that the equivalent MMC model with time-invariant solutions given in (2) has been validated against detailed models in [17] under common MMC controllers, and in [5] under the control structure investigated in this work.

## III. Particle Swarm Optimization Algorithm

The PSO algorithm, originally proposed in [14], is a simple and efficient heuristic search method which uses a set of particles to find the global minimum of an objective function. The method consists on first initializing the position of the particles, which are randomly distributed over the state space of interest. Then, the velocity of each of the particles, is updated at each iteration taking into account both the individual particles best result so far, as well as the best result of the whole swarm. Finally, the algorithm will usually come to an end after a certain number of iterations is reached. Although several versions of the algorithms have been proposed [13], this work is based on the implementation in [15], [16], and is summarized in the following lines.

1) The velocity and position of each particle are randomly initialized, typically within some bounds.
2) The objective function is evaluated using the current position of each of the particles.
3) The objective function value is *locally* compared with the individual particle's best result so far, say $c_l \in \mathbb{R}$. If the the current value is better than $c_l$, it becomes the new particle's local best. In addition, the particle's best position $\xi_l \in \mathbb{R}^p$ is updated with the current particle position.
4) The particle with the best $c_l$ out of the whole swarm is identified and compared with the swarm's *global* best result so far, say $c_g \in \mathbb{R}$. If this current global value is better than $c_g$, it becomes the swarm's new global best. In addition, the swarm best position $\xi_g \in \mathbb{R}^p$ is updated with the associated position.
5) Every particle's speed is updated according to $\psi_{k+1} = w\psi_k + \phi_1 R_1(\xi_l - \xi_k) + \phi_2 R_2(\xi_g - \xi_k)$, with $\psi_k \in \mathbb{R}^p$ and $\xi_k \in \mathbb{R}^p$ respectively the velocity and position of a particle corresponding to the iteration $k$, $\phi_{1,2}$ are acceleration constants, $R_{1,2} \in \mathbb{R}^{p\times p}$ are two diagonal matrices with its entries random numbers belonging to the set $[0, 1]$, and $w$ the inertia constant.
6) The position corresponding to each particle is updated according to $\xi_{k+1} = \xi_k + \psi_{k+1}$.
7) The steps 2) to 6) are repeated until $k$ reaches the maximum number of iterations specified by the user.

## IV. Control Structure under Investigation

The control structure under investigation is the PI-Passivity-based Control (PI-PBC) [11], [22], [23] applied to MMCs in a time-invariant framework, described in [6], [17]. This nonlinear control strategy based on passivity concepts [7], [10] with promising *plug-and-play* features is able to guarantee global asymptotic stability of the MMC. Although it is based on *linear* PI controllers, it is different from standard current control implementations since the PI is not wrapped around typical error signals, but instead around a signal called *passive output*. Due to its nonlinear nature, tuning methods based on linearisation and small-signal techniques will not necessarily guarantee a good performance of the system under large

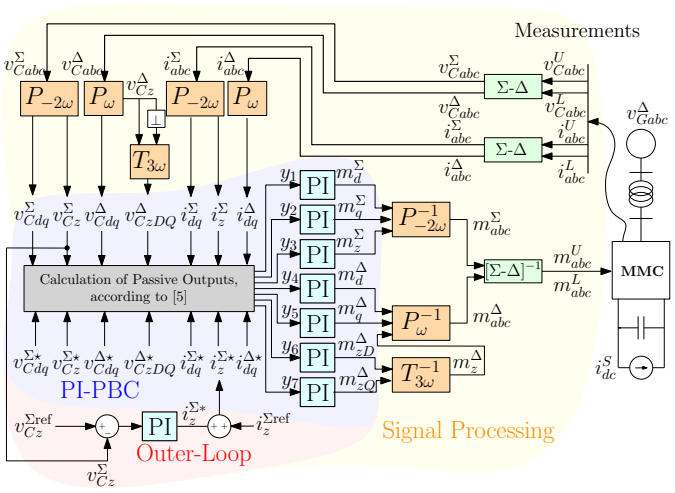


Fig. 4: Control diagram of an MMC in MT-HVDC configuration under PI-PBC+ $v_{Cz}^{\Sigma}$ outer-loop

disturbances. Thus, PSO appears as a good tuning method candidate for this application as it is able to take into account the system non-linearities introduced by the converter and its control.

Since, the MMC model under consideration given in (2) has seven control inputs; i.e., $u = \mathrm{col}(m_{dq}^{\Sigma}, m_{z}^{\Sigma}, m_{dq}^{\Delta}, m_{zDQ}^{\Delta}) \in \mathbb{R}^7$, it will have seven *passive outputs* as well, recalled in the appendix[1]. Thus, the control structure consists on seven *inner* PI controllers, each with their respective $K_P$, and $K_I$ coefficients, wrapped around each of the seven passive outputs—see Fig. 4. In addition, one *outer-loop* controller is introduced for robustness and dynamical improvements, as detailed in [5]. Thus, the PSO will be looking for the best PI coefficients of the PI-PBC method; i.e., the swarm's best position $\xi_g \in \mathbb{R}^{p=16}$.

## V. Simulation Results

This section presents some time-domain simulation results of a single-terminal MMC HVdc station under the PI-PBC + outer loop control strategy–depicted in Fig. 4 and summarized in section IV–and tuned with the PSO algorithm. The simulations have been carried out with the same system parameters used in [5], [6] and summarized in Table I. As mentioned earlier, we are interested in evaluating the performance of the PSO tuning methodology and its potential for coping with the nonlinearities naturally present in the MMC dynamical model and the chosen controller. Towards this end, we first investigate the effect of increasing each particle's vector dimension. Second, we examine the impact of using different objective functions in the PSO algorithm. Last but not least, we explore the outcome of increasing the PSO time limit, while evaluating the tuning performance under a large reference step.

[1]For a full derivation of the passive outputs corresponding to the MMC model given in (2), the interested reader is referred to [17].

TABLE I: MMC parameters

| | | | | | |
|---|---|---|---|---|---|
| $S_n$ | 1200 [MVA] | $N$ | 200 [-] | $C_\sigma$ | 21.16 [$\mu$F] |
| $U_n^{ac}$ | 380 [kV] | $R_f$ | 0.3429 [$\Omega$] | $R_\sigma$ | 0.6017 [$\Omega$] |
| $U_n^{dc}$ | 620 [kV] | $L_f$ | 62.9 [mH] | $L_\sigma$ | 30.6 [mH] |

### A. Effect of the increase of the particle vector dimension.

We are interested first in evaluating the effect of the increase of the particle vector dimension in the performance of the system. Therefore, the tuning parameters are obtained by the PSO methodology with different particle vector sizes, and the system response is evaluated thereafter. The particle composition and size is described in the following.

- `Case A`: This is the reference case where no PSO algorithm was used to tune the PI coefficients. More precisely, the PI coefficients are the same as those given in [5], [6].
- `Case B`: For this case, the PSO algorithm is used only to tune the PI coefficients of the outer-loop (OL) depicted in Fig. 4. Therefore, each particle is defined as $\xi_g \in \mathbb{R}^2$ with $\xi_g = \mathrm{col}(K_P^{\mathrm{OL}}, K_I^{\mathrm{OL}})$. [2]
- `Case C`: By contrast, in this case the PSO algorithm is used to tune all of the 16 PI coefficients present in the control structure under investigation—see Fig. 4. Thus each particle is defined $\xi_g \in \mathbb{R}^{16}$ with $\xi_g = \mathrm{col}(K_P^{\mathrm{OL}}, K_I^{\mathrm{OL}}, K_{P1}, \ldots, K_{P7}, K_{I1}, \ldots, K_{I7},)$.

The simulation event chosen is a reference step change of the (zero-sequence) of the MMC arm equivalent capacitor sum $v_{Cz}^{\Sigma}$—from 1.25 $pu$ to 1.35 $pu$. In addition, it is worth mentioning that the objective function used is one with the objective of minimizing the difference between the MMC state variables $x \in \mathbb{R}^n$ and their corresponding values in steady-state, of the form

$$V(x) = \sum_{i=1}^{n} q_{ii}||x_i - x_i^{\star}||^2 = (x - x^{\star})^{\top} Q (x - x^{\star}), \qquad (3)$$

with $x^{\star} \in \mathbb{R}^n$ denoting the equilibrium, and $Q = \mathrm{diag}(q_{ii}) \in \mathbb{R}^{n \times n}$ a diagonal matrix collecting the weighting factors $q_{ii}$.

The simulation results for the following three different cases are shown in Fig. 5, where we have chosen $Q$ to be the identity matrix for simplicity. Overall, the case where the PSO algorithm is used to tune all the PI coefficients (`Case C`) gives the best performance. In particular, it significantly improves the transitory peak of most of the variables without compromising too much on the settling time. The performance of the PSO algorithm search can be inferred from plotting the best value of the swarm $c_g$ with respect to each iteration. This is done for `Case B` and `Case C` in Fig. 5e and Fig. 5f, respectively. Although the algorithm is able to improve the converter performance only by means of the outer-loops, a re-tuning of all the coefficients clearly provides a significantly better result.

[2]We use $\mathrm{col}(a_i)$ to denote a column vector with entries $a_i$.

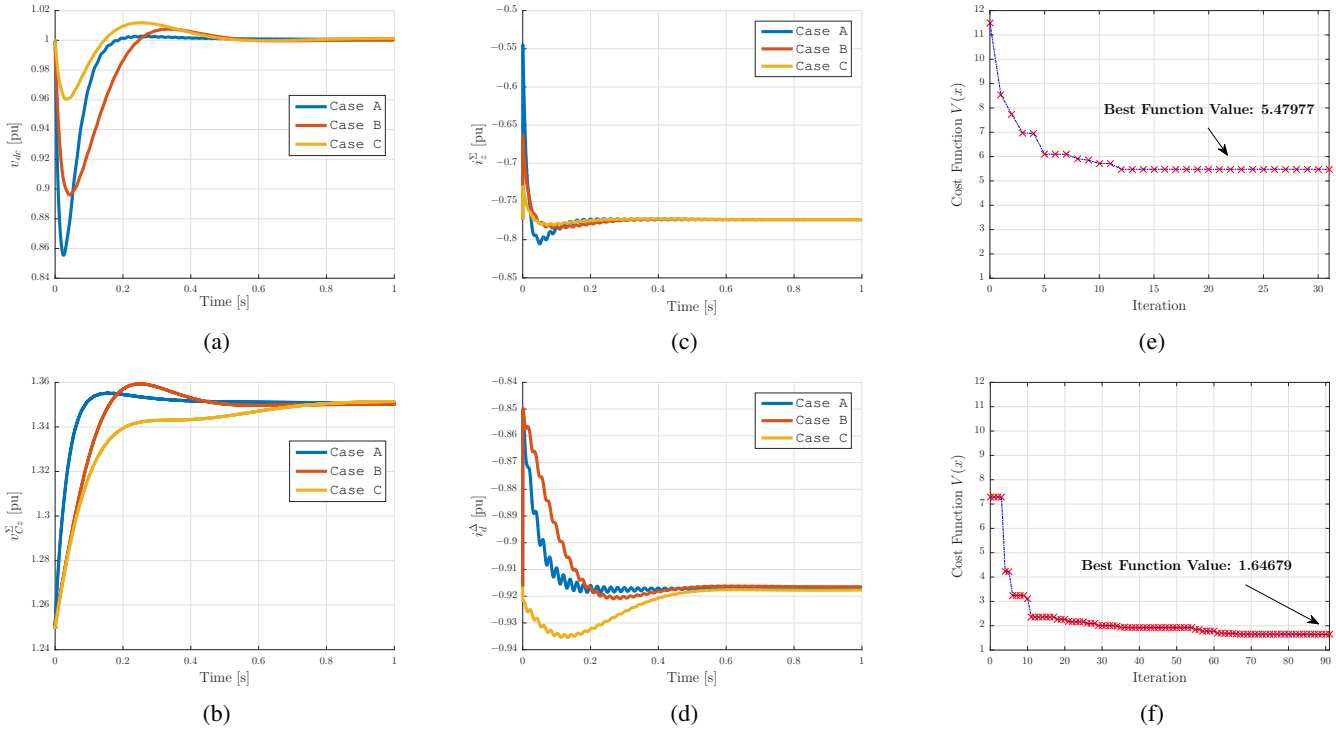


Fig. 5: Simulation results of (a) the voltage between the dc terminals $v_{dc}$, (b) the zero-sequence arm equivalent capacitor voltage sum $v_{Cz}^{\Sigma}$, (c) the zero-sequence of the circulating current $i_z^{\Sigma}$ and (d) the ac grid side active current $i_d^{\Delta}$, all under a step reference change of $v_{Cz}^{\Sigma\star}$ from 1.25 to 1.35 p.u.. In addition, the best value of the cost function at each iteration by applying PSO to (e) only the outer-loops (`Case B`) and (f) all the 16 PI coefficients (`Case C`).

### *B. Tuning performance with different PSO cost functions.*

We now turn to the evaluation of the effect that different objective functions in the PSO tuning algorithm have on the system dynamical behaviour. However, for the sake of simplicity, we maintain the *quadratic in the errors* structure of (3), and vary instead the weighting factors $q_{ii}$. The following objective functions are then evaluated, and the resulting dynamical performance is plotted in Fig. 6, under the same event detailed in section V-A.

- **ref.** This case denotes the reference scenario, where the diagonal weighting factor matrix $Q$ is simply the indentity matrix.
- **min $\boldsymbol{v_{Cz}^{\Sigma}}$.** This case gives priority to minimizing the error between the (zero-sequence) energy sum of the MMC and its steady-state value, by means of amplifying the effect of the error by a factor of 10 (i.e., $10 \cdot (v_{Cz}^{\Sigma} - v_{Cz}^{\Sigma\star})^2$).
- **min $\boldsymbol{i_{dq}^{\Delta}}$.** Similarly, this case gives priority to minimizing the error between the active and reactive ac grid currents and their desired steady-state value, by means of selecting a weighting factor of 10 (i.e., $10 \cdot (i_{dq}^{\Delta} - i_{dq}^{\Delta\star})^2$).

The waveform of the voltage sum $v_{Cz}^{\Sigma}$ is plotted in Fig. 6b. Clearly, the case corresponding to "**min $\boldsymbol{v_{Cz}^{\Sigma}}$**" has the fastest convergence rate of them all. This comes as no surprise as the objective function was formulated such that this convergence should have priority. Interestingly, however, this case under performs when we look at the other variables in Figs. 6a, 6c and 6d. More precisely, it causes the largest overshoots in the zero-sequence of the circulating current $i_z^{\Sigma}$ (proportional to the dc current) as well as in the voltage across the dc terminals of the converter $v_{dc}$—see Figs. 6c and 6a. In addition, it causes the most undamped oscillations in the ac grid active currents, as observed from Fig. 6d. By contrast, the case referred to as "**min $\boldsymbol{i_{dq}^{\Delta}}$**", not only produces the best performance in terms of the convergence of the active component of the grid current to its steady state–see Fig. 6d–but it also has good performance in terms of low overshoot and fast convergence in the variables $v_{dc}$ and $i_z^{\Sigma}$, depicted in Figs. 6a and 6c, respectively. Finally, the performance of the PSO algorithm is plotted here as well, for both objective functions; i.e., case "**min $\boldsymbol{v_{Cz}^{\Sigma}}$**" in Fig. 6e and case "**min $\boldsymbol{i_{dq}^{\Delta}}$**" in Fig. 6f. The best function values observed from these figures coincide with the above analysis in the sense that the case "**min $\boldsymbol{i_{dq}^{\Delta}}$**" gives an overall better performance.

### *C. Tuning performance with different PSO maximum time limits under a larger reference step.*

The objective of this section is twofold. First to investigate the capabilities of the PSO tuning methodology to cope with larger reference steps, and to evaluate the effect of increasing

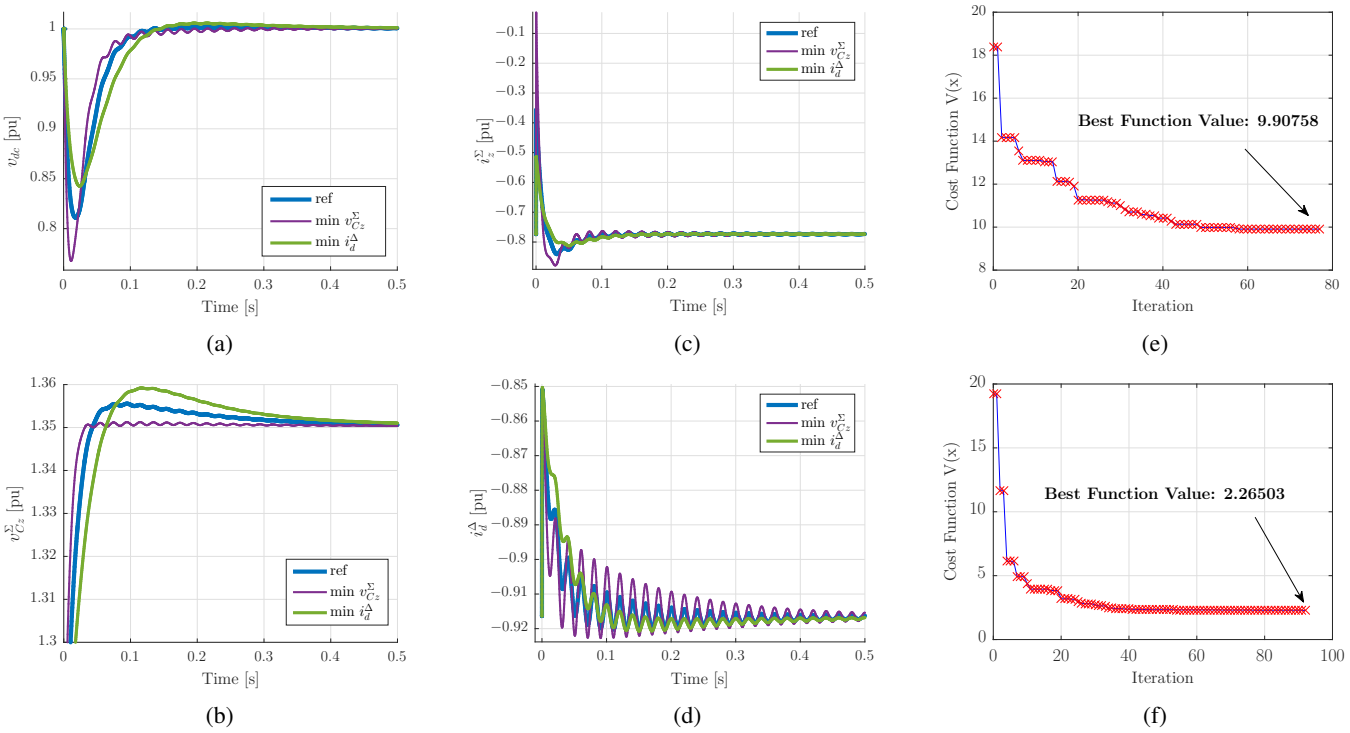


Fig. 6: Simulation results of (a) the voltage between the dc terminals $v_{dc}$, (b) the zero-sequence arm equivalent capacitor voltage sum $v_{Cz}^{\Sigma}$, (c) the zero-sequence of the circulating current $i_z^{\Sigma}$ and (d) the ac grid side active current $i_d^{\Delta}$, all under a step reference change of $v_{Cz}^{\Sigma\star}$ from 1.25 to 1.35 p.u. . In addition, the best value of the cost function at each iteration by applying PSO to (e) the case denoted as "**min** $v_{Cz}^{\Sigma}$" and (f) the case denoted as "**min** $i_d^{\Delta}$".

the searching time of the PSO algorithm. The reference step under consideration is a change of the dc current $i_{dc}^{S}$–see Fig 4–from $0.78$ to $-0.42$ in p.u., mimicking the event investigated in [5]. The waveform trends of the MMC variables of interest are depicted in Fig. 7. More precisely, the waveforms of the dc voltage $v_{dc}$, the MMC (zero-sequence) voltage sum $v_{Cz}^{\Sigma}$, the (zero-sequence) of the circulating current $i_z^{\Sigma}$ and the active component of the ac grid current $i_d^{\Delta}$, are respectively depicted in Figs. 7a, 7b, 7c and 7d. In such figures, the variables responses without the PSO tuning methodology (but instead with the tuning parameters used in [5]) are depicted, as well as their responses under the PSO tuning methodology using different maximum time limits; i.e., 5, 10 and 20 minutes.

As a first observation, we note that the method is able to ensure system stability under large reference steps, as the tuning is performed with the nonlinear model of the system. In addition, even though the PSO methodology improves the system behaviour in general, gains in performance do not significantly increase with the maximum allowed computation time. This can also be observed in the zoomed-in plots of $i_d^{\Delta}$ and $i_z^{\Sigma}$, respectively in Figs. 7e and 7f.

## VI. Conclusions

In this paper, we have explored the use of the Particle Swarm Optimization (PSO) algorithm as a tool for tuning the control coefficients of a nonlinear control strategy applied to the Modular Multilevel Converter (MMC) in a single-terminal HVdc configuration, able to ensure global asymptotic stability of the MMC.

The PSO methodology is able to cope with the nonlinear behaviour introduced by the converter and the control method of interest, as the tuning procedure avoid any linearization and is based instead on intensive time-domain simulations of the nonlinear model. Furthermore, in order to reduce the computational cost of the PSO, we propose to use a recently proposed equivalent average model of the MMC with time-invariant solutions–with $dqz$ coordinates–in the PSO tuning procedure. This allows to speed up the PSO algorithm, since initialization of the converter becomes possible and more efficient variable step solvers can be used.

Finally, we show via time-domain simulation results the positive effect that enlarging the size of the particle vector dimension has on the converter performance, as well as the converter response from different tunings in which we have modified the weighting coefficients in the PSO objective function.

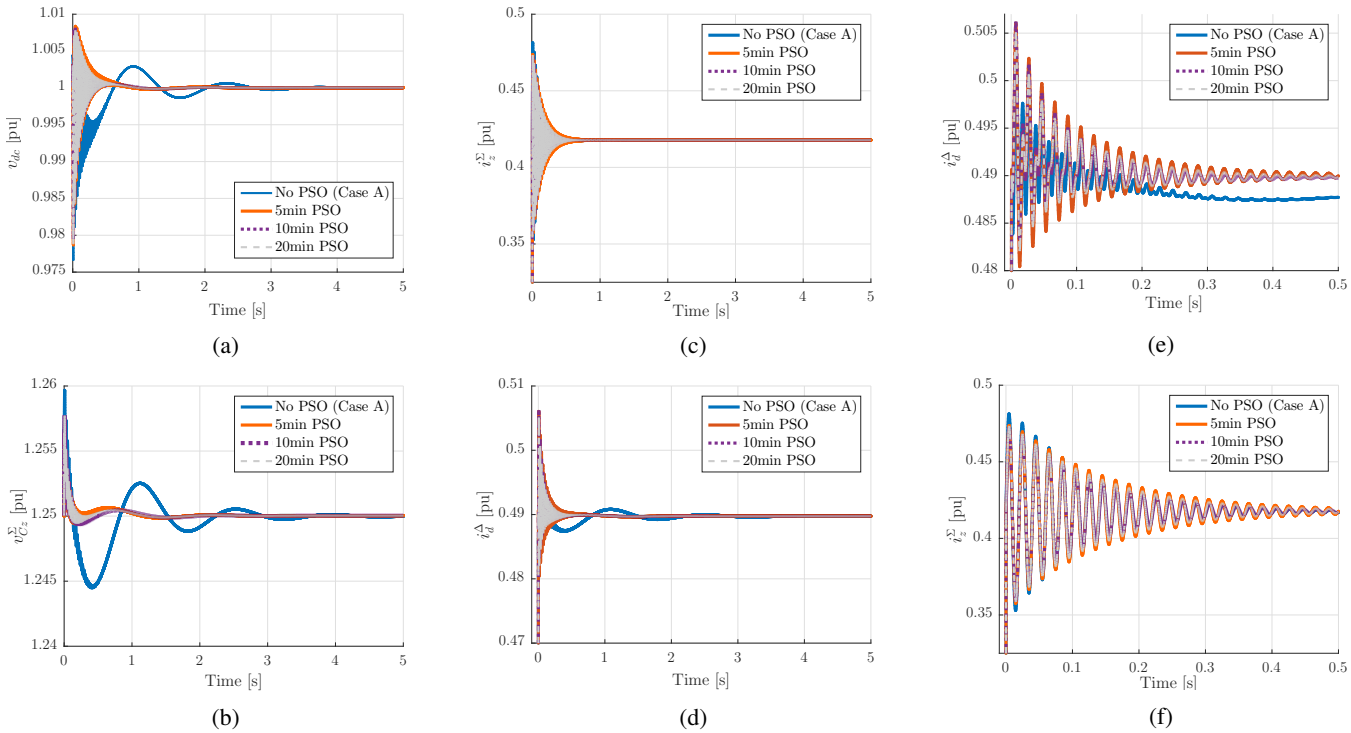


Fig. 7: Simulation results of (a) the voltage between the dc terminals $v_{dc}$, (b) the zero-sequence arm equivalent capacitor voltage sum $v^{\Sigma}_{Cz}$, (c) the zero-sequence of the circulating current $i^{\Sigma}_{z}$ and (d) the ac grid side active current $i^{\Delta}_{d}$, all under a step change of the dc current $i^{S}_{dc}$–see Fig 4–from 0.78 to $-0.42$ in p.u.. In addition, zoomed-in versions of the waveform responses are given for (e) $i^{\Delta}_{d}$ and (f) $i^{\Sigma}_{z}$.

## APPENDIX

The modulated currents and voltages appearing in (2) are defined according to [17], as:

$$i^{\Sigma}_{Mdqz} \triangleq P_{-2\omega}\left(P^{-1}_{-2\omega} m^{\Sigma}_{dqz} \circ P^{-1}_{-2\omega} i^{\Sigma}_{dqz} + P^{-1}_{\omega} m^{\Delta}_{dqz} \circ \frac{P^{-1}_{\omega} i^{\Delta}_{dqz}}{2}\right)$$

$$i^{\Delta}_{Mdqz} \triangleq P_{\omega}\left(P^{-1}_{\omega} m^{\Delta}_{dqz} \circ P^{-1}_{-2\omega} i^{\Sigma}_{dqz} + P^{-1}_{-2\omega} m^{\Sigma}_{dqz} \circ \frac{P^{-1}_{\omega} i^{\Delta}_{dqz}}{2}\right)$$

$$v^{\Sigma}_{Mdqz} \triangleq P_{-2\omega}\frac{P^{-1}_{-2\omega} m^{\Sigma}_{dqz} \circ P^{-1}_{-2\omega} v^{\Sigma}_{Cdqz} + P^{-1}_{\omega} m^{\Delta}_{dqz} \circ P^{-1}_{\omega} v^{\Delta}_{Cdqz}}{4}$$

$$v^{\Delta}_{Mdqz} \triangleq -P_{\omega}\frac{P^{-1}_{\omega} m^{\Delta}_{dqz} \circ P^{-1}_{-2\omega} v^{\Sigma}_{Cdqz} + P^{-1}_{-2\omega} m^{\Sigma}_{dqz} \circ P^{-1}_{\omega} v^{\Delta}_{Cdqz}}{4}$$

with $i^{\Sigma}_{Mdqz} \triangleq \mathrm{col}(i^{\Sigma}_{Mdq}, i^{\Sigma}_{Mz})$, $i^{\Delta}_{Mdqz} \triangleq \mathrm{col}(i^{\Delta}_{Mdq}, i^{\Delta}_{Mz})$ and $v^{\Sigma}_{Mdqz} \triangleq \mathrm{col}(v^{\Sigma}_{Mdq}, v^{\Sigma}_{Mz})$, $v^{\Delta}_{Mdqz} \triangleq \mathrm{col}(v^{\Delta}_{Mdq}, v^{\Delta}_{Mz})$.

The passive outputs of the MMC are computed according to [5] as:

$$\begin{aligned} y_1 =& \hat{i}^{\Sigma\star}_{z} v^{\Sigma}_{Cd} - \hat{i}^{\Sigma}_{z} v^{\Sigma\star}_{Cd} + \hat{i}^{\Sigma\star}_{d} \hat{v}^{\Sigma}_{Cz} - i^{\Sigma}_{d} \hat{v}^{\Sigma\star}_{Cz} + \hat{i}^{\Delta\star}_{d}\left(v^{\Delta}_{Cd} + v^{\Delta}_{CzD}\right) \\ & - \left(v^{\Delta\star}_{Cd} + v^{\Delta\star}_{CzD}\right)\hat{i}^{\Delta}_{d} + \hat{i}^{\Delta\star}_{q}\left(v^{\Delta}_{CzQ} - v^{\Delta}_{Cq}\right) \\ & - \left(v^{\Delta\star}_{CzQ} - v^{\Delta\star}_{Cq}\right)\hat{i}^{\Delta}_{q}, \\ y_2 =& \hat{i}^{\Sigma\star}_{z} v^{\Sigma}_{Cq} - v^{\Sigma\star}_{Cq} \hat{i}^{\Sigma}_{z} + i^{\Sigma\star}_{q} \hat{v}^{\Sigma}_{Cz} - \hat{v}^{\Sigma\star}_{Cz} i^{\Sigma}_{q} + \hat{i}^{\Delta\star}_{q}\left(v^{\Delta}_{Cd} - v^{\Delta}_{CzD}\right) \\ & - \left(v^{\Delta\star}_{Cd} - v^{\Delta\star}_{CzD}\right)\hat{i}^{\Delta}_{q} + \hat{i}^{\Delta\star}_{d}\left(v^{\Delta}_{Cq} + v^{\Delta}_{CzQ}\right) \\ & - \left(v^{\Delta\star}_{Cq} + v^{\Delta\star}_{CzQ}\right)\hat{i}^{\Delta}_{d}, \end{aligned}$$

$$\begin{aligned} y_3 =& \hat{i}^{\Sigma\star}_{d} v^{\Sigma}_{Cd} - v^{\Sigma\star}_{Cd} \hat{i}^{\Sigma}_{d} + i^{\Sigma\star}_{q} v^{\Sigma}_{Cq} - v^{\Sigma\star}_{Cq} i^{\Sigma}_{q} + \hat{i}^{\Delta\star}_{d} v^{\Delta}_{Cd} - v^{\Delta\star}_{Cd} \hat{i}^{\Delta}_{d} \\ & + \frac{1}{2}\left(\hat{i}^{\Sigma\star}_{z} \hat{v}^{\Sigma}_{Cz} - \hat{v}^{\Sigma\star}_{Cz} \hat{i}^{\Sigma}_{z}\right) + \hat{i}^{\Delta\star}_{q} v^{\Delta}_{Cq} - v^{\Delta\star}_{Cq} \hat{i}^{\Delta}_{q}, \\ y_4 =& \hat{i}^{\Delta\star}_{d}\left(v^{\Sigma}_{Cd} + \hat{v}^{\Sigma}_{Cz}\right) - \left(v^{\Sigma\star}_{Cd} + \hat{v}^{\Sigma\star}_{Cz}\right)\hat{i}^{\Delta}_{d} + \hat{i}^{\Delta\star}_{q} v^{\Sigma}_{Cq} - v^{\Sigma\star}_{Cq} \hat{i}^{\Delta}_{q} \\ & + i^{\Sigma\star}_{d}\left(v^{\Delta}_{Cd} + v^{\Delta}_{CzD}\right) - \left(v^{\Delta\star}_{Cd} + v^{\Delta\star}_{Cd}\right) i^{\Sigma}_{d} + \hat{i}^{\Sigma\star}_{z} v^{\Delta}_{Cd} \\ & - v^{\Delta\star}_{Cd} \hat{i}^{\Sigma}_{z} + i^{\Sigma\star}_{q}\left(v^{\Delta}_{Cq} + v^{\Delta}_{CzQ}\right) - \left(v^{\Delta\star}_{Cq} + v^{\Delta\star}_{CzQ}\right) i^{\Sigma}_{q}, \\ y_5 =& \hat{i}^{\Delta\star}_{q}\left(\hat{v}^{\Sigma}_{Cz} - v^{\Sigma}_{Cd}\right) - \left(\hat{v}^{\Sigma\star}_{Cz} - v^{\Sigma\star}_{Cd}\right)\hat{i}^{\Delta}_{q} + \hat{i}^{\Delta\star}_{d} v^{\Sigma}_{Cq} - v^{\Sigma\star}_{Cq} \hat{i}^{\Delta}_{d} \\ & + i^{\Sigma\star}_{q}\left(v^{\Delta}_{Cd} - v^{\Delta}_{CzD}\right) - \left(v^{\Delta\star}_{Cd} - v^{\Delta\star}_{CzD}\right) i^{\Sigma}_{q} + \hat{i}^{\Sigma\star}_{z} v^{\Delta}_{Cq} \\ & - v^{\Delta\star}_{Cq} \hat{i}^{\Sigma}_{z} + i^{\Sigma\star}_{d}\left(v^{\Delta}_{CzQ} - v^{\Delta}_{Cq}\right) - \left(v^{\Delta\star}_{CzQ} - v^{\Delta\star}_{Cq}\right) i^{\Sigma}_{d}, \\ y_6 =& \hat{i}^{\Delta\star}_{d} v^{\Sigma}_{Cd} - v^{\Sigma\star}_{Cd} \hat{i}^{\Delta}_{d} - \hat{i}^{\Delta\star}_{q} v^{\Sigma}_{Cq} - v^{\Sigma\star}_{Cq} \hat{i}^{\Delta}_{q} + i^{\Sigma\star}_{d} v^{\Delta}_{Cd} - v^{\Delta\star}_{Cd} i^{\Sigma}_{d} \\ & - i^{\Sigma\star}_{q} v^{\Delta}_{Cq} - v^{\Delta\star}_{Cq} i^{\Sigma}_{q} + \hat{i}^{\Sigma\star}_{z} v^{\Delta}_{CzD} - v^{\Delta\star}_{CzD} \hat{i}^{\Sigma}_{z}, \\ y_7 =& \hat{i}^{\Delta\star}_{q} v^{\Sigma}_{Cd} - v^{\Sigma\star}_{Cd} \hat{i}^{\Delta}_{q} + \hat{i}^{\Delta\star}_{d} v^{\Sigma}_{Cq} - v^{\Sigma\star}_{Cq} \hat{i}^{\Delta}_{d} + i^{\Sigma\star}_{q} v^{\Delta}_{Cd} - v^{\Delta\star}_{Cd} i^{\Sigma}_{q} \\ & + i^{\Sigma\star}_{d} v^{\Delta}_{Cq} - v^{\Delta\star}_{Cq} i^{\Sigma}_{d} + \hat{i}^{\Sigma\star}_{z} v^{\Delta}_{CzQ} - v^{\Delta\star}_{CzQ} \hat{i}^{\Sigma}_{z}. \end{aligned}$$

with the symbol $\star$ denoting the desired steady-state value at the equilibrium of the state variables. In addtion, $\hat{i}^{\Sigma}_{z} \triangleq 2i^{\Sigma}_{z}$, $\hat{v}^{\Sigma}_{Cz} \triangleq 2v^{\Sigma}_{Cz}$ and $\hat{i}^{\Delta}_{dq} \triangleq i^{\Delta}_{dq}/2$.

## ACKNOWLEDGMENT

This work was supported by the Norwegian Research Council and DNV-GL through the NFR contract n. 250493,

within the "Integrated Design and Control of Offshore HVDC Networks (IDeCON)" project.

## REFERENCES


[1] D. V. Hertem, O. Gomis-Bellmunt, and J. Liang, *IEEE Press Series on Power Engineering*. Wiley-IEEE Press, 2016, pp. 528–.

[2] A. Lesnicar and R. Marquardt, "An innovative modular multilevel converter topology suitable for a wide power range," in *Proc. IEEE Bologna Power Tech Conf.*, vol. 3, June 2003, p. 6.

[3] S. Rohner, S. Bernet, M. Hiller, and R. Sommer, "Modulation, losses, and semiconductor requirements of modular multilevel converters," *IEEE Trans. Ind. Electron.*, vol. 57, no. 8, pp. 2633–2642, Aug 2010.

[4] "Bestpaths EU project," http://bestpaths-project.eu/, accessed: 2017-06-26.

[5] G. Bergna-Diaz, D. Zonetti, S. Sanchez, R. Ortega, and E. Tedeschi, "PI passivity-based control and performance analysis of MMC multi-terminal HVdc systems," *IEEE Trans. Emerg. Sel. Topics Power Electron.*, pp. 1–1, 2018.

[6] G. Bergna-Diaz, D. Zonetti, S. Sanchez, E. Tedeschi, and R. Ortega, "PI passivity-based control of modular multilevel converters for multi-terminal HVdc systems," in *Proc. IEEE 18th Workshop Control Modeling Power Electron. (COMPEL)*, July 2017, pp. 1–8.

[7] H. K. Khalil, *Nonlinear systems*. Upper Saddle River, (N.J.): Prentice Hall, 1996.

[8] R. Ortega, A. van der Schaft, I. Mareels, and B. Maschke, "Putting energy back in control," *IEEE Control Syst. Mag*, vol. 21, no. 2, pp. 18–33, Apr 2001.

[9] V. Duindam, A. Macchelli, S. Stramigioli, and H. Bruyninckx, *Modeling and control of complex physical systems: the port-Hamiltonian approach*. Springer Science & Business Media, 2009.

[10] A. van der Schaft, *L2-Gain and Passivity in Nonlinear Control*, 2nd ed. Berlin, Heidelberg: Springer-Verlag, 1999.

[11] M. Hernandez-Gomez, R. Ortega, F. Lamnabhi-Lagarrigue, and G. Escobar, "Adaptive PI stabilization of switched power converters," *IEEE Trans. Control Syst. Technol.*, vol. 18, no. 3, pp. 688–698, May 2010.

[12] D. Zonetti, R. Ortega, and A. Benchaib, "Modeling and control of HVdc transmission systems from theory to practice and back," *Control Eng. Pract.*, vol. 45, pp. 133 – 146, 2015.

[13] K. Kameyama, "Particle swarm optimization - a survey," *IEICE Trans. Inform. Syst.*, vol. E92.D, no. 7, pp. 1354–1361, 2009.

[14] J. Kennedy and R. Eberhart, "Particle swarm optimization," in *Proc. IEEE Int. Conf. Neural Networks (ICNN)*, vol. 4, Nov 1995, pp. 1942–1948 vol.4.

[15] M. Calvini, M. Carpita, A. Formentini, and M. Marchesoni, "PSO-based self-commissioning of electrical motor drives," *IEEE Trans. Ind. Electron.*, vol. 62, no. 2, pp. 768–776, Feb 2015.

[16] Y. del Valle, G. K. Venayagamoorthy, S. Mohagheghi, J. Hernandez, and R. G. Harley, "Particle swarm optimization: Basic concepts, variants and applications in power systems," *IEEE Trans. Evol. Comput.*, vol. 12, no. 2, pp. 171–195, April 2008.

[17] G. Bergna-Diaz, J. Freytes, X. Guillaud, S. DArco, and J. A. Suul, "Generalized voltage-based state-space modeling of modular multilevel converters with constant equilibrium in steady state," *IEEE Trans. Emerg. Sel. Topics Power Electron.*, vol. 6, no. 2, pp. 707–725, June 2018.

[18] G. Bergna, J. A. Suul, and S. D'Arco, "State-space modelling of modular multilevel converters for constant variables in steady-state," in *Proc. IEEE 17th Workshop Control Modeling Power Electron. (COMPEL)*, June 2016, pp. 1–9.

[19] L. Harnefors, A. Antonopoulos, S. Norrga, L. Angquist, and H. P. Nee, "Dynamic analysis of modular multilevel converters," *IEEE Trans. Ind. Electron.*, vol. 60, no. 7, pp. 2526–2537, July 2013.

[20] H. Saad, X. Guillaud, J. Mahseredjian, S. Dennetière, and S. Nguefeu, "MMC capacitor voltage decoupling and balancing controls," *IEEE Trans. Power Del.*, vol. 30, no. 2, pp. 704–712, April 2015.

[21] G. Bergna-Diaz, J. A. Suul, and S. D'Arco, "Energy-based state-space representation of modular multilevel converters with a constant equilibrium point in steady-state operation," *IEEE Trans. Power Electron.*, vol. 33, no. 6, pp. 4832–4851, June 2018.

[22] M. Perez, R. Ortega, and J. Espinoza, "Passivity-based PI control of switched power converters," in *Proc. Eur. Control Conf. (ECC)*, Sept 2003, pp. 542–547.

[23] B. Jayawardhana, R. Ortega, E. Garcia-Canseco, and F. Castanos, "Passivity of nonlinear incremental systems: Application to PI stabilization of nonlinear RLC circuits," in *Proc. IEEE 45th Conf. Decision Control*, Dec 2006, pp. 3808–3812.